

# Asteroid Impacts and Their Geological Consequences



**Boris A. Ivanov**

The chapter reviews available data on the impact cratering in the Solar System. Most of data have been collected during robotic space missions to the Moon and other terrestrial planets. The brief introduction into the modern view on the planetary bombardment helps to present rationales for the impact cratering modeling. Morphology and morphometry of extraterrestrial impact craters, comparable in size with the Puchezh-Katunki structure illustrate that all these craters have clearly visible central mound. Crater's depth-diameter relations on planetary bodies with various surface gravity accelerations demonstrate that the simple-to-complex transitional crater diameter increases with decreasing of the surface gravity. The original depth of the Puchezh-Katunki structure and the presence of the central uplift well fit general trends, observed for impact craters on all planetary bodies of the terrestrial type.

## 1 General Information About Asteroid Impacts

The Puchezh-Katunki (PK) impact structure is one of thousands of impact craters found on Earth, the Moon and other planetary bodies. To immerse the PK description in a general context of impact cratering studies it is instructive to give a short review of main characteristics of known impact craters. The best introduction to the issue has been published by Melosh (1989). To model a crater, we need to assume the nature of the impactor body ("projectile" or "impactor"), its density and the impact velocity.

Many decades of the Solar System dynamics and evolution resulted in a "main-stream" concept, where most of Earth-striking projectiles arrive from the Main asteroid belt (MB). Asteroids normally rotate around the Sun on "safe" orbits, not crossing orbits of terrestrial planets. However, weak repetitive gravity forces (resonance

---

B. A. Ivanov (✉)

Institute for Dynamics of Geospheres, Leninsky Prospect 38-1, 117939 Moscow, Russia  
e-mail: [boris\\_a\\_ivanov@mail.ru](mailto:boris_a_ivanov@mail.ru)

forces) from giant planets like Jupiter and Saturn are able slowly change orbits of asteroids, and an asteroid orbit may become enough elliptical to cross orbits of terrestrial planets (Mercury, Venus, the Earth, and Mars). Collisions between asteroids also can slightly change asteroid orbits. Simultaneously, these collisions produce a number of fragments. Often these fragments are observed as asteroid families. Also, collisions slowly change the size-frequency distribution of small bodies in the MB. We can name these small bodies as “asteroid’s fragments”, or simply “small asteroids”.

The orbital motion of small asteroids and their rotation, in addition to gravity forces, may be changed with weak thermal radiation forces, generated by solar heating/cooling cycles. These effects (Yarkovsky effect, and Yarkovsky–O’Keefe–Radzievskii–Paddack effect, or YORP effect) depend on the body mass, and make small asteroid’s orbits more variable than for large asteroids. Gravity resonances and thermal radiation effects may act in chain—thermal radiation forces push a small body to the phase space position where resonances with giant planets act most effectively. The net effect is a permanent weak flux of small bodies from “safe” position to orbits, crossing planetary orbits, making collisions possible.

Being at planetary crossing orbits, small asteroids have relatively frequent flyby in locally strong planetary gravity fields. Close approaches occur much more often than planetary collision. Close approaches change planetary crossing orbits of small asteroids so that a single body cannot occupy the orbit infinitely. After  $\sim 3$  to  $\sim 30$  Myr a planetary crosser would fall to the Sun or will be accelerated to orbits beyond Jupiter. Hence, planetary-crossing asteroids observed now have low chances to impact the Earth, other asteroids would be delivered to similar orbits in a future.

It is less probable that a comet nuclear strike the Earth, as Jupiter-family comets originated from the Kuiper belt are observed at planetary-crossing orbits much less frequently than asteroids. Taking simple estimates of impact probabilities for known objects with diameters  $>1$  km (absolute magnitude  $H < 18$ ) we see that only  $\sim 5\%$  of these objects are on cometary-like orbits (Werner and Ivanov 2015). Parabolic and long periodic comets seems to have even smaller input to planetary impact bombardment during the last  $\sim 3$  Gyr—see the review by Dones et al. (2015).

Taking into account the most probable asteroid impact for the primary modeling, we use the known probability distribution to estimate impact velocity. Known  $H < 18$  terrestrial crossers occupy orbits giving the average impact velocity of  $19\text{--}20$  km  $\text{s}^{-1}$  (Werner and Ivanov 2015).

Density of asteroids is known from their fragments, falling to Earth as meteorites (Ostrowski and Bryson 2019). Space missions last decades delivered direct information about the bulk density of a set of asteroids. These estimates show that many asteroids have an appreciable porosity due to fracturing during their collisions with other asteroids (Scheeres et al. 2015). Most probable projectiles in the Earth/Moon system are S-type and C-type asteroids, with bulk densities of  $2000\text{--}3500$  kg  $\text{m}^{-3}$ . In the first approximation the reasonable initial modeling may be done assuming that the projectile is made of granite-like or basalt-like rocks.

## 2 Brief Introduction in Crater Mechanics Terminology

Briefly describing the impact cratering processes, we can conditionally split cratering in four distinct stages, differing in time length and in governing physical and mechanical processes. Following Melosh (1989), it is suitable to outline:

Stage 1—the contact and penetration phase. The projectile passes through the atmosphere and impacts the solid (or liquid) surface. At the contact point the shock wave is generated. The maximum pressure here is comparable with the projectile size.

Stage 2—shock wave propagation and the transient cavity growth. Shock wave propagates out of the contact zone, the shock front pressure decay with the propagation distance due to non-isoentropic compression/decompression (energy converts into residual heat) and due to geometrical divergence. After the shock wave passage material keep some residual velocity field out of the impact point. Rarefaction acoustic waves from the free target surface form so-called Z-model flow field, and roughly hemispheric or parabolic cavity starts to grow due to material displacement and ejection to the upper space. This cavity is named the “transient cavity”, as only in metals the shape of the final crater is close to the transient cavity shape at the end of its evolution.

Stage 3—the transient cavity modification. The size of the transient cavity is controlled by two main target parameters—gravity field and rock strength. The target material, deforming around the growing transient cavity, experiences the strength resistance, and convert part of its initial kinetic energy into the mechanical “plastic” work. Simultaneously, the flow field, opening the transient cavity by the material displacement uplift the material up in the planetary gravity field, converting the kinetic energy into the potential energy. Part of the flow field energy is lost as the ejecta kinetic energy. The balance between the total “plastic” work against rock strength, and the total potential energy define the so-called cratering regime: if plastic work is the main energy sink, we define that the transient crater is formed in a “strength-dominated” regime. In the alternative case, when the most of the initial flow field kinetic energy is converted into potential energy, we define, that the transient crater is formed in a “gravity-dominated” regime. In a widespread slang we name these cases as “gravity” and “strength” craters.

In dependence on the cratering regime type, a transient cavity, when it reaches the maximum volume, modifies the shape in various ways. First, in strong ductile materials like metals or plasticine, the transient cavity is simply “frozen” with strength forces. Second, in brittle materials, where fragmented rocks behave as a dry sand with the internal friction, a part of cratering walls may slide down to the crater bottom, forming so-called “breccia lens”. And third, the residual strength of material around the transient cavity may be low enough to start the collapse of the cavity when the crater floor begins to move up, like the central jet in a water cavity after a pebble dropped to a pond. This case is discussed later in the Section [“Computation and Geological Data”](#).

Here we need to state that on all planetary surfaces we see two distinct types of craters—craters, modified mostly by wall slopes are named “simple” craters, and craters, where we see the transient crater uplift, are named “complex” craters.

The floor uplift in complex craters may be hidden under the breccia lens. In this case only depth/diameter ratio comparison may reveal the started floor uplift. We can define these craters as “transitional” from simple to complex. For larger craters the central uplift may be visible as a central peak or peak ring. Largest impact basins have a multiring structure.

Stage 4—the post-impact crater evolution is mostly a set of geologic processes changing the shape of a just-formed impact crater. For large craters these processes include impact melt motion before a final solidification, heat conduction and hot fluids convection to establish a new thermal regime around the new crater. On other planets the post-impact evolution includes as an important part the ongoing bombardment by smaller objects. And, of course, large craters, as adjacent areas, are modified with “normal” endogenic process like tectonics, volcanism, denudation, and sedimentation.

### 3 Large Impact Craters on Earth and Other Planetary Bodies

Space missions delivered images of surface on Mercury, Venus, the Moon, Mars, largest asteroids Ceres and Vesta, a dozen of small asteroids. For beyond the asteroid belt objects images are taken for Pluto/Chiron, large satellites of giant planets, for a few of comet nuclei, and, recently, for one of Kuiper belt objects. With rare exception (i.e. Io, Jupiter satellite with the global volcanic activity), all planetary surfaces are covered with impact craters, demonstrating that impact cratering is one of the main processes, formed and renovating solid surfaces of planets and their satellites. Many extraterrestrial planetary bodies have endogenic geologic processes less active than on Earth, or stopped to operate billions years ago. As the result, craters on other planetary bodies often show more pristine impact crater morphology than we see on Earth.

**The Moon** is studied with multiple space missions, including astronaut’s landing and sample return. The absence of atmosphere allows even dust particles to collide the lunar surface without any deceleration. For this reason, we observe lunar impact craters in wide range of sizes—from micron-size craters from micrometeorite impacts to impact basins with 1000 km diameters.

Figure 1 illustrates crater morphologies for a simple, a transitional and, a complex crater. The simple crater has a bowl shape with a small breccia patch at the floor. The transitional crater has irregular floor, but no visible central feature. The complex crater has a flat floor with the central mound. To outline crater shape differences, crater profiles (North to South) are shown in Fig. 2 in coordinates, scaled to a crater rim diameter. In the ideal case, crater rim should be placed at  $x/D = \pm 0.5$ . Irregular

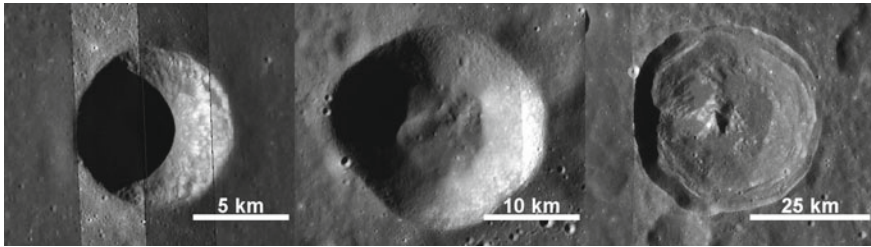


**Fig. 1** Typical examples of a simple crater (left,  $D \sim 8$  km, unnamed 359.17E, 8.52S), a transitional crater (center,  $D \sim 20$  km, unnamed, 26.385 E, 39.95 S) and a complex (right,  $D \sim 40$  km 357.859 E, 5.656 S) Hershel crater. Images are generated with the public JMars software (<https://jmars.asu.edu/>) and based on the LROC WAC mosaic. The left image is enhanced with overlapped LROC images M1188368973LC and M1188368973RC

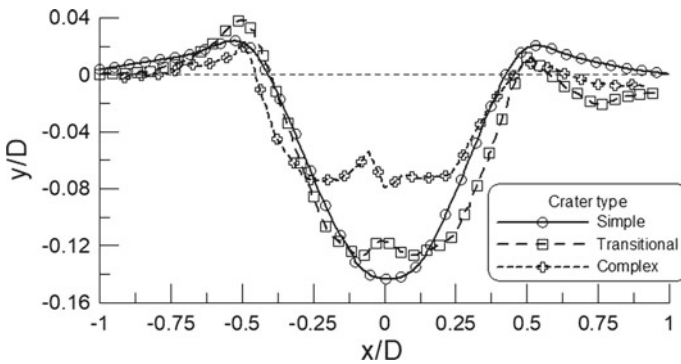


**Fig. 2** North-south topographic profiles through three craters, shown in Fig. 4.1. Profiles are constructed with the public JMars software and based on LOLA 1024 ppd (point per degree) topographic map

lunar surface makes hard to find the pre-impact ground level; an approximate position  $y = 0$  is shown with a dashed line. The scaled plot well illustrates how a crater depth to diameter ratio,  $d/D$ , decreases at the transition from simple to complex craters.

A set of papers presents the statistics of  $d/D$  variation with size. First Apollo-era measurements of the lunar crater depth revealed that simple craters are self-similar in a shape, and their  $d/D$  ratio is close to 0.2 in a wide crater diameter range from 100 m to 15 km (Pike 1977). The constant  $d/D$  means that the crater depth increases linearly with diameter:

$$d \approx 0.2D \tag{1}$$

This is close to crater depth in laboratory high-velocity impact experiments with dry sand, and this fact additionally approves the term “simple” craters (Schmidt and Housen 1987). One should note, that small lunar craters ( $D < 1$  to 2 km) degrade

faster than larger craters (Ivanov 2018), and below  $D \sim 1$  km we observe shallow degraded craters with depths below Eq. 1 (Stopar et al. 2017). Here Eq. 1 is valid only for fresh craters.

In a gravity cratering regime (see Section “[Brief Introduction in Crater Mechanics Terminology](#)”), crater rim profiles should be similar in shape—all measurable values like depth and rim height should be linearly proportional to the crater rim diameter (Housen et al. 1983). However, there is no final opinion at which diameter lunar craters change the strength formation regime to the gravity regime. The only one paper by Moore et al. (1974) mentioned explicitly  $D \sim 300$  m as the effective strength/gravity transition diameter. However, the problem seems to be connected to a non-uniform character of the lunar surface. The upper layer is a regolith, underlined with fragmented rock/soil mixture with rock fragment size and percentage increasing with depth (Heiken et al. 1991). Cohesion and dry friction could vary with depth. Intuitively it seems reasonable to assume that lunar rocks become more competent with depth. If so, there is not a single strength/gravity crater regime transition. It is a matter of a future study to understand how strength and gravity interplay in a wide range of crater diameters. A good introduction in the problem is the numerical modeling study of the strength/gravity transition in uniform targets by Prieur et al. (2017).

The simplest quantitative characteristic of the simple/complex crater transition is given with measurements of the crater depth,  $d$ , growth with the crater diameter,  $D$ . For the Moon the function  $d(D)$  has been measured in 1970s, and these measurements continue now with better elevation measurements at the lunar surface. First systematic measurements are published by Pike (1977), and recent papers sufficiently improve Pike’s data (Kalynn et al. 2013; Stopar et al. 2017; Krüger et al. 2018; Osinski et al. 2019). Figure 3 illustrates the current understanding of the lunar  $d(D)$  function.

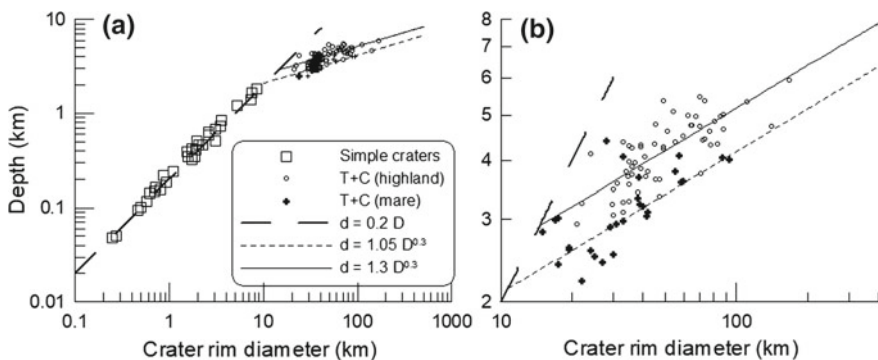


**Fig. 3** Rim-to-floor lunar crater depth as a function of the crater diameter. Data for simple craters are from (Stopar et al. 2017). Data for transitional (T) and complex (C) craters are from (Kalynn et al. 2013). Approximated exponent relations (solid, dashed, and dotted curves) are plotted to give a guide to the data cloud and not correspond to statistical method. For power law regression see primary publications. (a) The whole crater diameter range, (b) The blowup for complex craters

A reader should take into account relatively large uncertainties for large crater measurements. The roughness of the lunar surface and crater rim crest irregularity results in individual depth values from 0.1 to 2 km—see, for example, Fig. 3 in Kalynn et al. (2013). Without any first principle theory, we prefer to illustrate the general trends in  $d(D)$  for transitional and complex craters with simple power laws, based on primary vision of Pike (1977). Figure 3 illustrates general trends in  $d(D)$  with simple relations ( $d$  and  $D$  are measured in km):

for lunar mare

$$d = 1.05D^{0.3} \quad (2a)$$

for lunar highlands

$$d = 1.3 D^{0.3} \quad (2b)$$

These simple power relations cross the  $d(D)$  dependence (1) at  $D = 10.7$  km on mare, and  $D = 14.5$  km on highlands. We can take these values as a primary estimate for the simple/complex crater transition. The exhaustive review about  $d(D)$  approximations for all cratered planetary bodies is published by Robbins et al. (2018).

Looking at the crater morphology, we see a more complex pattern—transitional craters have no visible central peak, but have lower  $d/D$  in comparison with a simple crater dependence (1). So morphologic transition to fully developed central peak craters is extended in the  $D$  range from  $\sim 15$  to  $\sim 30$  km (Krüger et al. 2018).

The reason to have slightly different  $d(D)$  trends for mare and highland craters seems to result from local differences in strength parameters in different locations (Osinski et al. 2019). Lunar highlands present an ancient lunar crust, significantly fragmented by the continuous impact bombardment (megaregolith). Lunar mare are multiple basaltic flows, deposited over the same megaregolith. Osinski et al. (2019) believe that layered basaltic flow structures on mare result in relatively small target rock cohesion, reflected in smaller  $d(D)$  for complex craters. The problem needs more quantitative study in a future.

On other planetary bodies we observe similar  $d(D)$  relations, complicated with local differences between surface composition, gravity acceleration and presence of an atmosphere. In general, the behavior of  $d(D)$  is the same as on the Moon—approximately similar dependence for simple craters as (1), and less steep  $d$  growth for complex craters (2018). Within goals of this chapter we outline the main feature of the interplanetary  $d(D)$  relations, namely—the increase of an effective crater diameter of simple/complex crater,  $D_{sc}$ , at bodies with smaller gravity acceleration at the surface.

**Venus** has the surface gravity acceleration, close to the terrestrial one ( $8.07$  vs.  $9.81 \text{ ms}^{-2}$ ) but much denser atmosphere and higher surface temperature (Ivanov et al. 1986, 1992; Phillips et al. 1991, 1992). The dense atmosphere plays a two-fold role: (1) meteoroid's breakup at the atmospheric entry disrupts high-velocity projectiles, and (2) dense atmosphere could affect the process of ejecta from the transient cavity. As the result we do not find simple deep craters as on the Moon—a single small

body cannot reach the surface, and small craters on Venus are presented with crater clusters. In many cases a body could start fragmentation and fragment separation at low altitudes, resulting in a crater formation by a swarm of fragments (Cochrane and Ghail 2006). Consequently, we have no simple craters to compare them directly with simple lunar craters.

The comparison of Venusian and terrestrial large craters is very important due to a similar value of the surface gravity acceleration. However we should compare these craters with some caution, as the dense Venusian atmosphere could change the ejecta deposition pattern near a crater rim (Ivanov et al. 1992; Schultz 1992; Ivanov 2008).

Surface images of Venus are available after synthetic-aperture radar (SAR) missions Venus 15/16 and Magellan. Dense Venusian atmosphere is opaque for visible light, so radar reflections are processed to produce images as variations of reflected signals mainly due to surface roughness and dielectric properties of surface rocks. Morphology of craters, comparable in size with Puchezh-Katunki is exemplified in Fig. 4.

Impact craters found on Venus have been measured with radar image distortion techniques (Ivanov 1989; Sharpton 1994), with simple altimetric signals (Ivanov and Ford 1993), and later, after detailed processing of radar images with different incidence angle, with constructed digital terrain models (DTM)—see Herrick et al. (2012). Figure 5 presents the best available crater depth/diameter data for Venus in comparison with terrestrial craters.

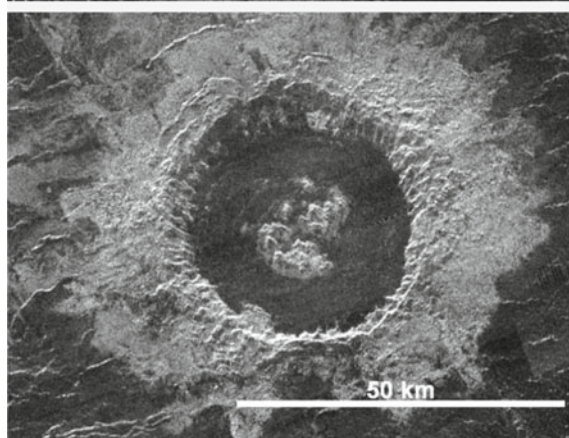
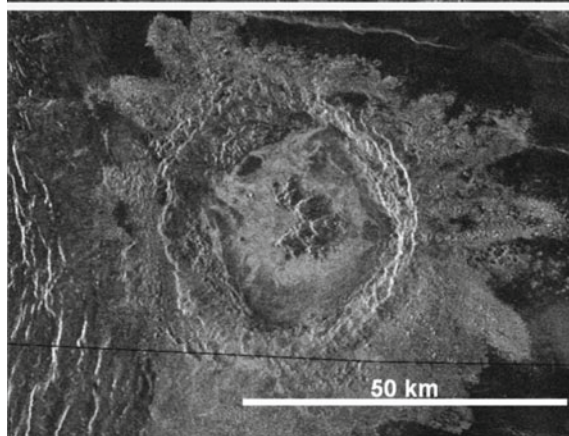
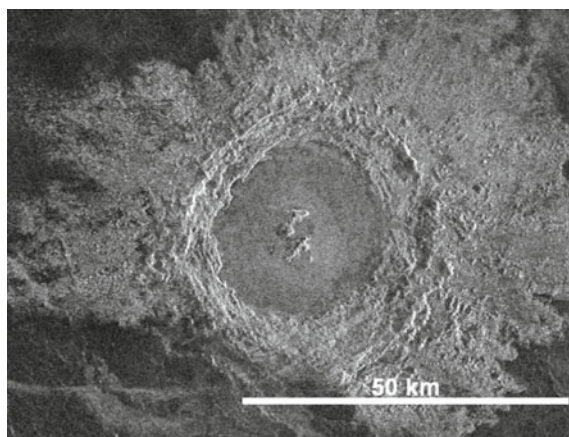
Figure 4 illustrates that on Venus, a rocky planet with the gravity, close to the terrestrial one, craters with  $D \sim 40$  km have the same morphological type as the Puchezh-Katunki impact structure. Venusian craters have a flat floor, central mounds, and terraced inner crater slopes. Despite the dense atmosphere, Venusian craters have a clear visible zone of ejecta depositions beyond the crater rim. Due to high target surface temperature (737 K, i.e. 462 °C) high-velocity impacts produce more impact melt than it would be on Earth. More important is that the impact melt on Venus is more mobile due to slower cooling by hotter rock fragments (Ivanov et al. 1992). This longer melt mobility could explain the smooth (radar-dark) appearance of Venusian crater floors.

The depth trend in complex crater depths both for Venus and for Earth (Fig. 5) may be presented with the lunar-like power law

$$d = 0.3D^{0.3} \quad (3)$$

giving at  $D = 40$  km the crater depth of 0.9 km, what is much less than for lunar craters of the same diameter (3–4 km). This difference illustrates how gravity forces control the transient cavity collapse during a complex impact crater formation. The closeness of Venusian and terrestrial  $d(D)$  trends illustrates a weak dependence on a water presence. The lower depth of terrestrial craters in sedimentary targets could indicate as the lower material strength, as well as a participation of water in the strength lowering.





◀**Fig. 4** Three Venusian craters with diameters close to the Puchezh-Katunki impact structure: Xiao Hong (left,  $D \approx 38.7$  km), La Fayette (middle,  $D \approx 39.6$  km) and Duncan (right,  $D \approx 40.3$  km). The visible brightness of the central mound, inner crater walls and continuous ejecta zone are mainly resulted from the enhanced surface roughness, contrasted with smooth (radar-dark) plains outside craters and impact melt pond surface inside. Magellan mosaic F-BIDRs, (Full resolution Basic Image Data Records  $\sim 75$  m/pixel). Publisher: USGS Astrogeology Science Center. Images are generated with JMars software (<https://jmars.asu.edu/>)

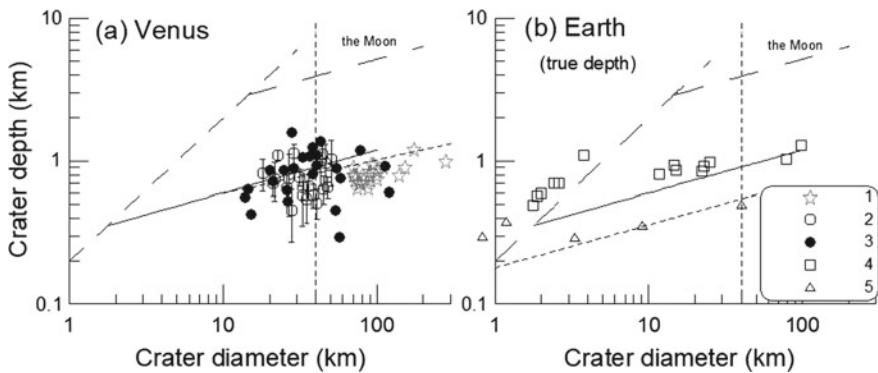


**Fig. 5** Available crater depth estimates for Venus (a) and Earth (b). 1—direct altimeter measurements (Ivanov and Ford 1993), 2—DEM (Neish et al. 2017), 3—DEM (Cochrane and Ghail 2006). Terrestrial data (b) are illustrated with “true” crater depths collected by Grieve et al. (1981) for craters in crystalline (4) and sedimentary rock targets. Note that data points (2, 3) include rim heights into rim-to-floor depth, while data points (1) on Venus and (3, 4) on Earth presents so called “terrain-to-floor” depth, i.e. the crater floor depth below an estimated pre-impact surface level. Long-dashed curves (lines in the log-log plot) present lunar data (Fig. 4.3). Solid curves trough data clouds are not fitting lines and are drawn with the same power law as on Fig. 4.3 ( $d \sim D^{0.3}$ ) to fit the data at  $D \sim 40$  km to compare later the “depth deficit” versus a hypothetical simple crater on different planetary bodies. The vertical dotted line shows approximately the Puchezh-Katunki diameter

**Mercury and Mars.** Another pair of planetary bodies with close surface gravity accelerations, but different near-surface geology is Mercury ( $g = 3.7 \text{ m s}^{-2}$ ) and Mars ( $g = 3.72 \text{ m s}^{-2}$ ). Morphology of simple craters here changes with a crater diameter in the same way as on the moon—from simple craters to complex craters with central uplifts (Fig. 6).

For the comparison we plot on Fig. 6 lunar-like curves (lines in log-log coordinates) for complex crater’s  $d(D)$ :

$$D = 0.75 * D^{0.3} \tag{4}$$

for Mercury and

$$D = 0.8 * D^{0.3} \tag{5}$$

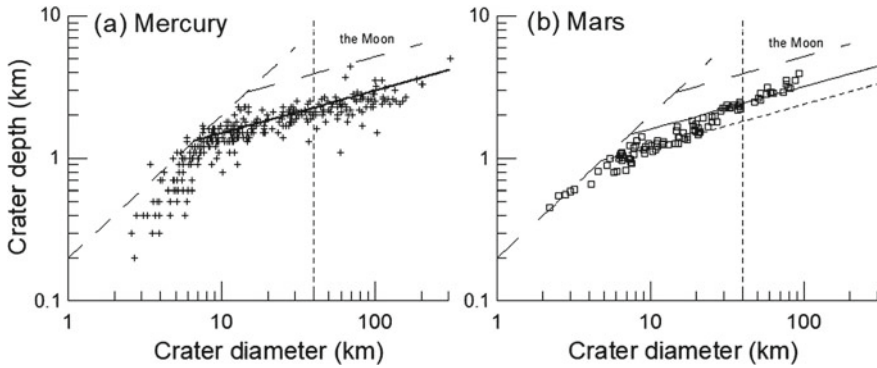


**Fig. 6** Available data on the depth/diameter,  $d(D)$ , relations for impact craters measured on Mercury (a) and Mars (b). Long dashed curves (lines in log-log coordinates show lunar  $d(D)$  trends for simple and complex craters. Data for Mercury are collected by Susorney et al. (2016), and for Mars by (Tornabene et al. 2018). The vertical dotted line shows approximately the Puchezh-Katunki diameter

for Mars.

Here we do not want to discuss the visible deflection of  $d(D)$  from Eq. 5, and simply plot the curve (5) to cross measured data around  $D = 40$  km.

Images of two impact craters on Mercury and on Mars with diameters near 40 km are shown in Fig. 7.

Craters with sizes, close to the Puchezh-Katunki impact structure, on all five planetary bodies have similar morphology: relatively flat floor with the central mound. The shape of central mounds slightly varies even at the same planetary body, exemplified with Venusian craters in Fig. 4. It seems to reflect local difference in target

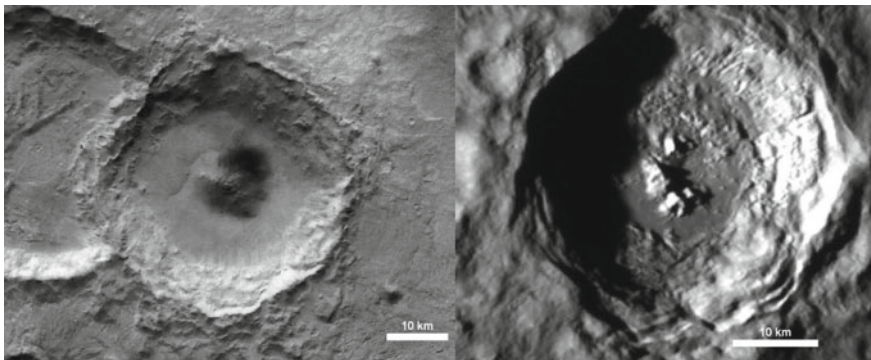


**Fig. 7** Complex impact craters with diameters 38 km on Mars (left) and on Mercury (right). Mars coordinates are 118.2 E, 39.5 S, HRSC image H8728\_0000\_ND3. Mercury coordinates are 122.03 E, 10.0 S, MDIS image EN1016060659 M. Images are generated with JMars software (<https://jmars.asu.edu/>)

**Table 1** The depth estimates for a crater with  $D = 40$  km on terrestrial planetary bodies

Planetary body	Gravity acceleration, $g, \text{m s}^{-2}$	Crossing diameter <sup>a</sup> $D_*$ (km)	Crater depth (km)
Moon mare highlands	1.62	10.7	3.2
		14.5	3.9
Mars	3.71	7.2	2.4
Mercury	3.7	6.6	2.3
Venus	8.9	1.8	0.9
Puchezh-Katunki (Earth)	9.81	–	0.8–1.5

<sup>a</sup>The diameter where  $d(D)$  trends for complex craters cross the trend for simple craters (see Figs. 3, 5, and 6)

properties, but some researches connect this difference with a possible effects of different impact velocities (Osinski et al. 2019).

Crater depths for complex craters (in most cases—the depth of a flat floor around the central mound) systematically vary with the crater diameter, growing much slower than  $d(D)$  for simple craters. Theoretically the value  $d/D$  for complex craters depends on the ratio  $D/D_{sc}$ , where  $D_{sc}$  is the simple-to-complex transitional diameter (Croft 1985; Wünnemann and Ivanov 2003). The value of  $D_{sc}$  increases with the decrease of the gravity acceleration, e.g. Pike (1980) suggested that  $D_{sc} \sim g^{-1}$ . Recent data, including impact craters on icy bodies, demonstrates a possibility of a slightly less strong dependence on  $g$  (Hiesinger et al. 2016), and this issue still demands more analysis. For a practical comparison with the Puchezh-Katunki structure we use approximations with the lunar-like  $d(D)$  slope to trace how the depth for  $D = 40$  km crater varies from the Moon to Venus (Table 1). As the gravity acceleration raises up, the diameter of an effective transition from simple to complex crater's  $d/D$  decreases from  $D_* \sim 15$  km to  $D_* \sim 2$  km, and the crater depth decreases from 3 to 4 km on the Moon to  $\sim 1$  km on Venus.

The presence of the central uplift in the Puchezh-Katunki structure and its estimated pristine depth about 0.8 to 1.5 km (with the uncertainty where was the crater floor just after impact) make the structure a typical impact crater of its size on terrestrial planets in our Solar System.

## References

- Cochrane CG, Ghail RC (2006) Topographic constraints on impact crater morphology on Venus from high-resolution stereo synthetic aperture radar digital elevation models. *J Geophys Res Planets* 111:E04007. <https://doi.org/10.1029/2005JE002570>
- Croft SK (1985) The scaling of complex craters. *J Geophys Res* 90:C828–C842
- Dones L, Brassier R, Kaib N, Rickman H (2015) Origin and evolution of the cometary reservoirs. *Space Sci Rev* 197:191–269

- Grieve RAF, Robertson PB, Dence MR, Schultz PH (1981) Constraints on the formation of ring impact structures, based on terrestrial data. In: Merrill RB (ed) *Multi-ring basins: formation and evolution*. Pergamon Press, New York and Oxford, pp 37–57
- Heiken GH, Vaniman DT, French BM (1991) *Lunar sourcebook—a user's guide to the moon*. Cambridge University Press, Cambridge, UK, p 753
- Herrick RR, Stahlke DL, Sharpton VL (2012) Fine-scale venusian topography from magellan stereo data. *Eos, Trans Am Geophys Union* 93(12):125–126
- Hiesinger H, Marchi S, Schmedemann N, Schenk P, Pasckert JH, Neesemann A, O'Brien DP, Kneissl T, Ermakov AI, Fu RR, Bland MT, Nathues A, Platz T, Williams DA, Jaumann R, Castillo-Rogez JC, Ruesch O, Schmidt B, Park RS, Preusker F, Buczkowski DL, Russell CT, Raymond CA (2016) Cratering on Ceres: implications for its crust and evolution. *Science* 353(6303):aaf4759
- Housen KR, Schmidt RM, Holsapple KA (1983) Crater ejecta scaling laws—fundamental forms based on dimensional analysis. *J Geophys Res* 88:2485–2499
- Ivanov BA (1989) The morphometry of impact craters on Venus. *Astronomicheskii Vestnik* 23:39–49 (in Russian)
- Ivanov B (2008) Impact cratering on venus: ballistic hole in the atmosphere (abs.). In: *Proceedings European planetary science congress 2008*, Münster, Germany, p 341
- Ivanov BA (2018) Size-frequency distribution of small lunar craters: widening with degradation and crater lifetime. *Sol Syst Res* 52(1):1–25
- Ivanov BA, Ford PG (1993) The depths of the largest impact craters on Venus. *Lunar and Planetary Science XXIV*. Houston, TX, pp 689–690
- Ivanov BA, Bazilevsky AT, Krivchikov VP, Chernaia IM (1986) Impact craters of venus—analysis of venera 15 and 16 data. *J Geophys Res* 91:D413–D430
- Ivanov BA, Nemchinov IV, Svetsov VA, Provalov AA, Khazins VM, Phillips RJ (1992) Impact cratering on Venus: Physical and mechanical models. *J Geophys Res* 97(E10):16167–16181
- Kalynn J, Johnson CL, Osinski GR, Barnouin O (2013) Topographic characterization of lunar complex craters. *Geophys Res Lett* 40:38–42
- Krüger T, Hergarten S, Kenkmann T (2018) Deriving morphometric parameters and the simple-to-complex transition diameter from a high-resolution, global database of fresh lunar impact craters ( $D \geq 3$  km). *J Geophys Res Planets* 123:2667–2690
- Melosh HJ (1989) *Impact cratering—a geologic process*. Oxford University Press, Oxford—New York, p 245
- Moore HJ, Hodges CA, Scott DH (1974) Multiringed basins—illustrated by orientale and associated features. In: *Proceedings 5th lunar and planetary science conference*, Pergamon Press, New York, pp 71–100
- Neish CD, Herrick RR, Zanetti M, Smith D (2017) The role of pre-impact topography in impact melt emplacement on terrestrial planets. *Icarus* 297:240–251
- Osinski GR, Silber EA, Clayton J, Grieve RAF, Hansen K, Johnson CL, Kalynn J, Tornabene LL (2019) Transitional impact craters on the moon: insight into the effect of target lithology on the impact cratering process. *Meteorit Planet Sci* 54:573–591
- Ostrowski D, Bryson K (2019) The physical properties of meteorites. *Planet Space Sci* 165:148–178
- Phillips RJ, Arvidson RE, Boyce JM, Campbell DB, Guest JE, Schaber GG, Soderblom LA (1991) Impact craters on venus—initial analysis from Magellan. *Science* 252:288–297
- Phillips RJ, Raubertas RF, Arvidson RE, Sarkar IC, Herrick RR, Izenberg N, Grimm RE (1992) Impact craters and venus resurfacing history. *J Geophys Res* 97:15923–15948
- Pike RJ (1977) Size-dependence in the shape of fresh impact craters on the moon. In: Roddy DJ, Pepin RO, Merrill RB (eds) *Impact and Explosion Cratering: Planetary and Terrestrial Implications*. Pergamon Press, Oxford, pp 489–509
- Pike RJ (1980) Control of crater morphology by gravity and target type—Mars, Earth, Moon. In: *Proceedings of the eleventh Lunar and Planetary Science Conference*, pp 2159–2189
- Prieur NC, Rolf T, Luther R, Wünnemann K, Xiao Z, Werner SC (2017) The effect of target properties on transient crater scaling for simple craters. *J Geophys Res Planets* 122(8):2017JE005283

- Robbins SJ, Watters WA, Chappelow JE, Bray VJ, Daubar IJ, Craddock RA, Beyer RA, Landis M, Ostrach LR, Tornabene LL, Riggs JD, Weave BP (2018) Measuring impact crater depth throughout the solar system. *Meteorit Planet Sci* 53:583–637
- Scheeres DJ, Britt D, Carry B, Holsapple KA (2015) Asteroid Interiors and Morphology. In: Michel P, DeMeo FE, Bottke FW (eds) *Asteroids IV*. University of Arizona Press, Tucson, pp 745–766
- Schmidt RM, Housen KR (1987) Some recent advances in the scaling of impact and explosion cratering. *Int J Impact Eng* 5:543–560
- Schultz PH (1992) Atmospheric effects on ejecta emplacement and crater formation on Venus from Magellan. *J Geophys Res* 97(E10):16183–16248
- Sharpton VL (1994) Evidence from Magellan for unexpectedly deep complex craters on Venus. In: Dressier BO, Grieve RAF, Sharpton VL (eds) *Large Meteorite Impacts and Planetary Evolution*. Geological Society of America, Boulder, CO, pp 19–27
- Stopar JD, Robinson MS, Barnouin OS, McEwen AS, Speyerer EJ, Henriksen MR, Sutton SS (2017) Relative depths of simple craters and the nature of the lunar regolith. *Icarus*. <https://doi.org/10.1016/j.icarus.2017.05.022>
- Susorney HCM, Barnouin OS, Ernst CM, Johnson CL (2016) Morphometry of impact craters on Mercury from MESSENGER altimetry and imaging. *Icarus* 271:180–193
- Tornabene LL, Watters WA, Osinski GR, Boyce JM, Harrison TN, Ling V, McEwen AS (2018) A depth versus diameter scaling relationship for the best-preserved melt-bearing complex craters on Mars. *Icarus* 299:68–83
- Werner SC, Ivanov BA (2015) Exogenic dynamics, cratering, and surface ages (chapter 10.10). In: Schubert G (ed) *Treatise on geophysics*, 2nd edn. Elsevier, Oxford, pp 327–365
- Wünnemann K, Ivanov BA (2003) Numerical modelling of the impact crater depth–diameter dependence in an acoustically fluidized target. *Planet Space Sci* 51(13):831–845